



Optics Letters

Dual modality reflection mode optical coherence and photoacoustic microscopy using an akinetic sensor

RICHARD HAINDL,¹ STEFAN PREISSER,¹ MARCO ANDREANA,¹ WOLFGANG ROHRINGER,²
CATERINA STURTZEL,³ MARTIN DISTEL,³ ZHE CHEN,¹ ELISABET RANK,¹ BALTHASAR FISCHER,²
WOLFGANG DREXLER,¹ AND MENG YANG LIU^{1,*}

¹Center for Medical Physics and Biomedical Engineering, Medical University of Vienna, Währinger Gürtel 18-20, 1090 Vienna, Austria

²Xarion Laser Acoustics, GmbH, Ghegastraße 3, 1030 Vienna, Austria

³Innovative Cancer Models, Children's Cancer Research Institute, Zimmermannplatz 10, 1090 Vienna, Austria

*Corresponding author: mengyang.liu@meduniwien.ac.at

Received 30 August 2017; revised 20 September 2017; accepted 25 September 2017; posted 26 September 2017 (Doc. ID 306075); published 18 October 2017

This Letter presents a novel dual modality reflection mode optical coherence and photoacoustic microscopy (OC-PAM) system. The optical coherence microscopy modality features a broadband source to accomplish 5 μm axial resolution. The photoacoustic microscopy modality uses a rigid akinetic Fabry–Perot etalon encapsulated in an optically transparent medium, which forms a 2 mm \times 11 mm translucent imaging window, permitting reflection mode dual modality imaging. After characterization, the OC-PAM system was applied to image zebrafish larvae *in vivo*, demonstrating its capability in biomedical imaging with complementary optical scattering and absorption contrasts by revealing morphology in the fish larvae. © 2017 Optical Society of America

OCIS codes: (120.2230) Fabry-Perot; (170.4500) Optical coherence tomography; (170.5120) Photoacoustic imaging.

<https://doi.org/10.1364/OL.42.004319>

Provided under the terms of the [OSA Open Access Publishing Agreement](#)

Dual modality optical imaging combining optical coherence microscopy (OCM) and photoacoustic microscopy (PAM) has been proven to provide complementary contrasts in biological tissues in a non-invasive manner, thus permitting promising applications in preclinical studies [1]. Among all the configurations to realize optical coherence and photoacoustic microscopy (OC-PAM), most of them use piezoelectric ultrasound transducers for acoustic wave detection [2–18]. While commercially available and relatively easily customizable, the opaque transducers pose challenges when incorporating OCM into PAM [19]. In transmission mode OC-PAM configurations using piezoelectric transducers, a water tank may be required [3,9,12,13], limiting its application to thin specimens. In reflection mode, in most cases, an unfocused transducer needs to be positioned obliquely with respect to the optical axis,

causing sensitivity loss [2,4,5,7,11,14–16,18]. Thus, it is beneficial to investigate alternative configurations permitting reflection mode OC-PAM.

With the various applications in which OC-PAM has been demonstrated valuable, such as in ophthalmology [4,7,11,14] and in metabolic rate measurement [5,11], most efforts in technical innovations for OC-PAM were made in utilizing a single light source for both OCM and PAM [8,9,16,17]. As for OC-PAM using optical detection of acoustic waves, a low coherence interferometry method was employed to detect the phase change on a sample surface, which is induced by photoacoustic waves [20–22]. While this method brings non-contact OC-PAM into the field, surface vibration detection using an interferometer requires stringent phase stability from the excitation laser source. Furthermore, the success of the technique depends on the surface topography and requires control of reflections in order to guarantee effective interference in the fiber coupler.

Besides optical detection PAM methods employing a Michelson [20,21] or Mach–Zehnder [22] interferometer for dual modality OC-PAM systems, there are several types of PAM realizations using alternatives to piezoelectric transducers for detection. Such methods include optical detection using a Fabry–Perot interferometer (FPI) in the form of a polymer film sensor [23–25], micro-ring resonator detection [26], and low-power non-contact air-coupled microphone detection [27]. However, these methods still require or involve mechanical deformation for acoustic pulse detection. The most recent optical detection solutions such as polarization-dependent optical reflection sensing [28] and photoacoustic remote sensing [29] hold promising prospects for OC-PAM, but they either require intricate optical alignment or lack depth information.

One way to use an FPI in photoacoustic imaging is the detection of the refractive index modulation caused by the photoacoustic wave. A prototype sensor working under this

principle has been demonstrated to have flat frequency response, a large field of view and a noise equivalent (NEP) pressure of $450 \mu\text{Pa}/\sqrt{\text{Hz}}$, corresponding to 2 Pa when normalized to 20 MHz bandwidth [30]. In this Letter, a modified design of the akinetic sensor featuring a large translucent imaging window and a thickness of only 1 mm was used for dual modality OC-PAM. After characterization, the novel dual modality system was applied to image zebrafish larvae *in vivo*, demonstrating its potential in biomedical settings.

Figure 1(a) shows the schematic of the reflection mode OC-PAM system. A broadband superluminescent diode (Broadlighter T840, Superlum) with a central wavelength of 840 nm and a bandwidth of 107 nm were used as the OCM source. The fiber optic system featured a 90/10 beam splitter from which 10% of the light was guided to the sample arm. After being emitted from the collimator, the beam was reflected on a dichroic mirror (DMLP650, Thorlabs) before incidence upon a microscope objective (UPlanSApo 4x, Olympus). The light power at the position of the sample was measured to be $230 \mu\text{W}$. In the reference arm, a dispersion compensating prism pair and the same objective as in the sample arm were used for dispersion compensation. The homemade spectrometer consisted of a transmission grating with 1200 lines/mm (3253-W-01, Wasatch Photonics), a focusing lens (85 mm $f/2.0$ Makro-Planar T, Zeiss), and a line scan camera (Sprint spl4096, Basler) operating at 10 kHz.

The PAM part of the system used a 532 nm pulsed laser (SPOT 10-200-532, Elflorlight) operating at 50 kHz repetition rate with 1 ns pulse duration. The pulse energy was attenuated to 50 nJ at the position of the sample to stay way below the damage threshold for biological samples [31]. During the measurement, the control unit (Eta L Hydrophone, XARION) used an interrogation laser in the telecom range to continuously probe the akinetic sensor. Different from the previous version [30], where the stability at optimum bias can be lost due to minor perturbations, the newly built control unit incorporates an automatic optimum bias tracking function, which monitors optimum bias drift in real time and tunes the interrogation laser wavelength accordingly. This feature significantly loosened the requirement for ambient environment such as temperature change and vibration. The photoacoustically modulated

intensity change of the probe light reflected from the etalon was monitored, amplified, and conditioned before the signal was sent to the data acquisition card (ATS9350, Alazar Technologies), which was synchronized with the excitation laser.

The scanning unit depicted in Fig. 1(b) is composed two parts. The first part employed two 1D stages to hold the sample and the akinetic sensor, respectively. Figure 1(c) gives a top view sketch of the sensor. It shows the exact dimension of the sensor along with the probing beam. The sensor is glued to a hollow tube through whose lumen the fiber delivering the probing light is inserted. The tip of the fiber has a collimator, through which the probing beam propagates into the FPI cavity. The second part was the raster scanning unit, which was mounted on top of two orthogonally positioned linear actuators (T-LSM05A, Zaber Technologies). Limited by the stepping speed of the linear actuators, an A-line rate of 1000 A-lines/min can be achieved without averaging.

Characterization results of the akinetic sensor are given in Fig. 2. The effective imaging area for PAM was measured by placing a cover glass with uniform black paint directly below the akinetic sensor and then raster scanning the excitation beam over an area of $2 \text{ mm} \times 12 \text{ mm}$, which is larger than the effective imaging area of the sensor. The boundary of the effective imaging area was set at pixels with a signal-to-noise ratio (SNR) of 4, which can be calculated using Fig. 2(c). The PAM sensitivity roll-off was calculated by gradually changing the distance between the akinetic sensor and the sample, while keeping the sample at the focal point of the excitation beam. The lateral resolutions of the OC-PAM system were measured by placing a United States Air Force resolution target under the akinetic sensor and scanning through a sharp edge of one element. Then the edge and line spread functions were calculated, and the latter one was fitted to a Gaussian curve. The full width at half-maximum of the fitted curve was taken as the resolution value. A summary of the specifications of the OC-PAM system is given in Table 1. The slightly better lateral resolution in OCM compared to PAM is because of the objective which is configured for near infrared. The deviation from the theoretical OCM axial resolution is due to a combination of several factors such as the non-uniform quantum efficiency of the CMOS line detector, the spectrometer objective (designed

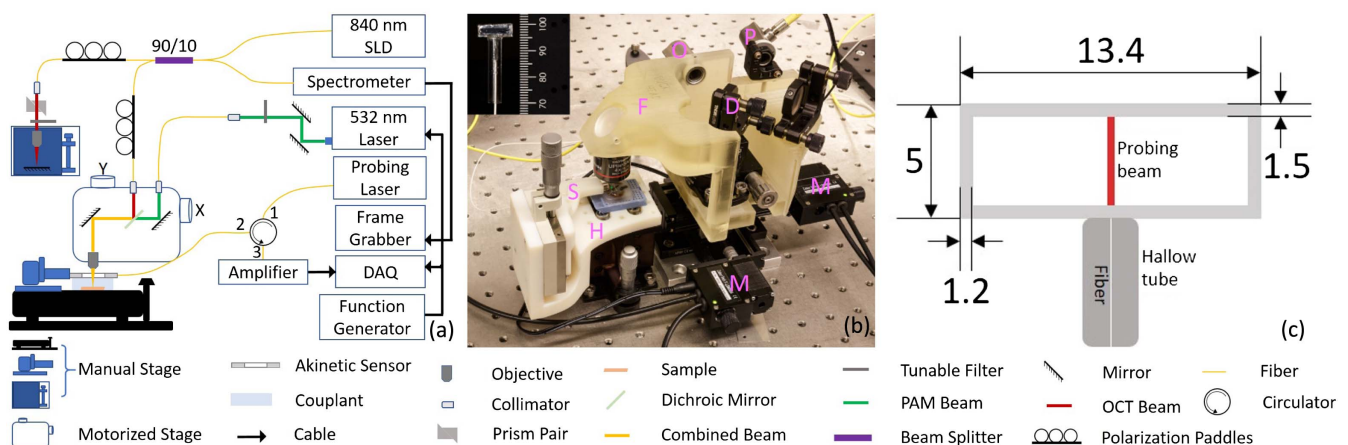


Fig. 1. (a) Schematic of the reflection mode OC-PAM system. (b) Photo of the scanning unit (inset, photo of the akinetic sensor). S, sensor holder; H, holder for sample; M, motorized stage; D, dichroic mirror; P, collimator for PAM; O, collimator for OCM; F, framework for the scanning unit. (c) Drawing of the sensor (unit, mm).

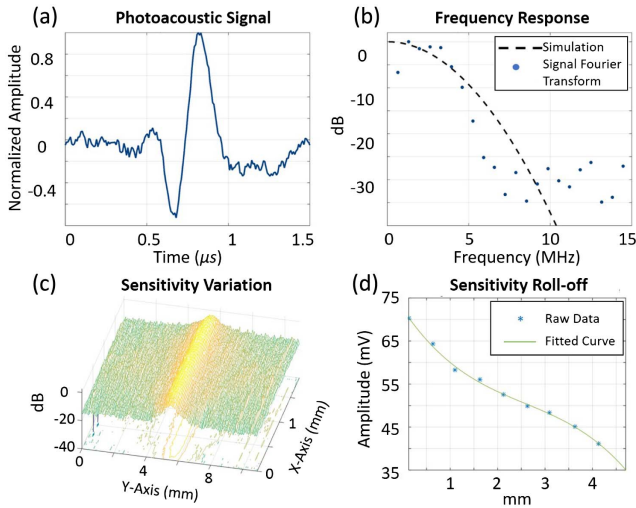


Fig. 2. (a) Typical photoacoustic signal captured by the PAM subsystem. (b) Simulated frequency response and the Fourier transform of the signal given in (a). (c) Effective imaging area expressed in sensitivity variation. (d) Sensitivity roll-off of the akinetic sensor over depth.

for visible wavelengths), and bandwidth losses in the beam splitter and optical fiber.

To demonstrate the complementary capability of the OC-PAM system in biomedical applications, 1-phenyl 2-thiourea (PTU) treated wild type zebrafish larvae, anesthetized in tricaine and embedded in agar, were imaged. We applied some ultrasound gel on top of the agar for acoustic coupling. Limited by the stepping speed of the actuators, the total imaging time might take several hours considering the number of points to be scanned in one session.

The OC-PAM system worked in sequential mode for the two modalities. Such a configuration was preferable, since a wavelength (and objective)-dependent focal shift occurred between the two modalities. We plan to incorporate a Keplerian telescope in the PAM excitation path to co-register the foci of the two modalities [16].

As was presented in [32], which used a piezoelectric ultrasound transducer to image zebrafish larvae in transmission mode, the akinetic sensor in our OC-PAM system was able to resolve absorbing structures in the samples such as pigment cells, and structures in the yolk sac, the heart, and the retinal pigment epithelium (RPE), which can be seen in Fig. 3(b). The axial vein and dorsal aorta of the PTU treated wild type zebrafish larvae are partly occluded with pigment cells and, therefore, were not clearly identifiable. In the future, *mitfa*^{b692/b692},

ednrba^{b140/b140} (AB) zebrafish, which lack pigmentation, will help overcome this difficulty and enhance the visibility of the vascular system.

From Figs. 3(a) and 3(c), we can see that the OCM modality provides details of the zebrafish larval morphology such as the eye, the swim bladder, and the otic vesicle with otoliths. From Figs. 3(d)–3(f), the advantage of our high axial resolution in OCM and intrinsic depth gating is well exhibited in resolving the structural changes of the eye over several hundred micrometers. The lens, the RPE, and some other surrounding structures in the larvae are well discernible over the depth range.

To show the potential of fast scanning over a large area in reflection mode using PAM, we have set up a separate PAM system using galvanometer scanning mirrors. The principle of the separate system stays the same as that of the PAM part in the OC-PAM system. The only difference is the use of scanning mirrors. During imaging, the sample, the sensor, and the optical components stay static, except for the scanning mirrors. Some preliminary results are given in Fig. 4, showing the chromophore distribution in three different types of zebrafish larvae.

Unlike the results given in [32], intersegmental vessels are not visible in PAM maximum amplitude projection (MAP) images in Fig. 3. However, with a faster imaging speed using scanning mirrors to replace the motorized stages, we have properly resolved the intersegmental vessels as are given in Fig. 4. We believe that this is because of the shorter amount of time needed using the scanning mirrors (from hours to 13 min), which reduced motion artifacts significantly. Another reason could be that some of the fish larvae did not survive the hour-long imaging session in the stage-based system while, in the scanning-mirror-based system, their survival rate is guaranteed which, in turn, gives a better signal in blood vessels. Currently, we have a stage-based OC-PAM system and a fast scanning PAM system. We are now upgrading the latter system further to incorporate the OCM modality into the fast scanning system.

The 6 dB bandwidth of 3.5 MHz is insufficient to achieve depth sectioning due to the limited axial resolution in the PAM mode. However, a 22 MHz akinetic prototype sensor has

Table 1. Specifications of the OC-PAM System

OCM	PAM	
Sensitivity	98 dB (10 kHz)	530 $\mu\text{PA}/\sqrt{\text{Hz}}$ (NEP)
Axial roll-off	10 dB/mm	0.67 dB/mm
Axial resolution	5 μm	286 μm
Lateral resolution	3 μm	4 μm
Frequency response	—	3.5 MHz (-6 dB)
Effective imaging area	22 mm^2	21 mm^2

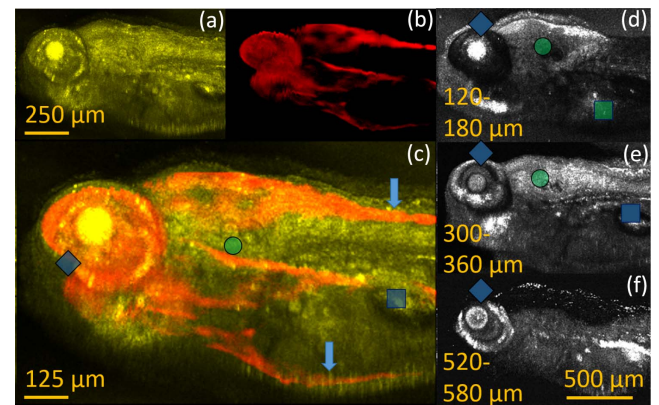


Fig. 3. Images of a 120 h post-fertilization (hpf) zebrafish larva. (a) Maximum intensity projection (MIP) image of OCM. (b) MAP image of PAM. (c) Color blended OC-PAM image using (a) and (b). (d)–(f) MIP images of OCM integrating 60 μm depth range. Blue arrow, pigments; blue square, swim bladder; blue diamond, eye; green circle, vesicle with otoliths; green square, yolk sac.

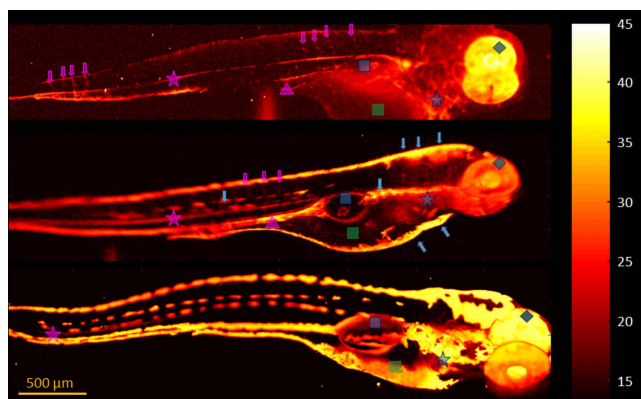


Fig. 4. PAM comparison between 120 hpf larvae from differently pigmented zebrafish strains using fast scanning PAM. The color bar shows the SNR in decibels. Upper image, *mitfa*^{b692/b692}, *ednra*^{b140/b140} (AB) zebrafish, PTU treated; middle image, wild type AB* zebrafish, PTU treated; lower image, Tg(Fli:GFP) zebrafish. Blue arrows, pigment; blue square, swim bladder; blue diamond, eye; blue star, heart; magenta star, dorsal aorta; tip of magenta triangle, axial vein; magenta arrows, intersegmental vessels; green square, yolk sac.

already been demonstrated with a smaller imaging window [30]. For a sensor with a large imaging window, the probing beam needs to maintain a narrow waist to achieve a broader acoustic detection bandwidth, which is challenging in cavity design. We are now investigating the possibility of using miniaturized concave mirrors for the cavity to replace the flat mirrors. In theory, this can increase the bandwidth by an order of magnitude.

With a higher bandwidth, we conceive that the akinetic sensor can operate in a reflection mode OC-PAM system without the necessity to use averaging to resolve finer complementary details in biological samples. The ensuing speed increase will enable dual modality fast scanning with functional extensions. Among them, spectroscopic extensions using a dye laser will enable the measurement of blood oxygenation. With the addition of Doppler OCM, the dual modality system can determine the metabolic rate of oxygen in blood vessels. These functional extensions will be particularly useful and beneficial in biological studies relating to tumor growth and drug dynamics.

To the best of our knowledge, we present the first reflection mode OC-PAM system featuring a novel akinetic sensor for photoacoustic detection with a large effective imaging area. The detection principle relies on the acoustically modulated refractive index change inside the FPI cavity. With the sample and the sensor both being static, we achieved *in vivo* scanning over a large imaging area with good sensitivity and lateral resolution. The complementary contrasts provided by OCM and PAM were illustrated by imaging zebrafish larvae. We aim for the implementation of spectroscopic reflection mode fast scanning functional OC-PAM. This approach will significantly enhance the scope of both modalities to provide relevant physiological information for a variety of biomedical studies.

Funding. Österreichische Forschungsförderungsgesellschaft (FFG) (5035366, 855797); The European Union Projects, Seventh Framework Programme (FP7) Information and Communication Technologies (ICT) (317744); Horizon 2020 Framework Programme (H2020) (732720).

Acknowledgment. We thank Keith Oakes at Elforlight for servicing the PAM excitation source.

REFERENCES

- W. Drexler, M. Liu, A. Kumar, T. Kamali, A. Unterhuber, and R. A. Leitgeb, *J. Biomed. Opt.* **19**, 071412 (2014).
- S. Jiao, Z. Xie, H. F. Zhang, and C. A. Puliafito, *Opt. Lett.* **34**, 2961 (2009).
- L. Li, K. Maslov, G. Ku, and L. V. Wang, *Opt. Express* **17**, 16450 (2009).
- S. L. Jiao, M. S. Jiang, J. M. Hu, A. Fawzi, Q. F. Zhou, K. K. Shung, C. A. Puliafito, and H. F. Zhang, *Opt. Express* **18**, 3967 (2010).
- T. Liu, Q. Wei, J. Wang, S. Jiao, and H. F. Zhang, *Biomed. Opt. Express* **2**, 1359 (2011).
- X. Cai, Y. Zhang, L. Li, S.-W. Choi, M. R. MacEwan, J. Yao, C. Kim, Y. Xia, and L. V. Wang, *Tissue Eng., Part C* **19**, 196 (2013).
- W. Song, Q. Wei, T. Liu, D. Kuai, J. M. Burke, S. Jiao, and H. F. Zhang, *J. Biomed. Opt.* **17**, 061206 (2012).
- X. Zhang, H. F. Zhang, and S. Jiao, *J. Biomed. Opt.* **17**, 030502 (2012).
- C. Lee, S. Han, S. Kim, M. Jeon, M. Y. Jeon, C. Kim, and J. Kim, *Appl. Opt.* **52**, 1824 (2013).
- V. Tsytarev, B. Rao, K. I. Maslov, L. Li, and L. V. Wang, *J. Neurosci. Methods* **216**, 142 (2013).
- W. Song, Q. Wei, W. Liu, T. Liu, J. Yi, N. Sheibani, A. A. Fawzi, R. A. Linsenmeier, S. Jiao, and H. F. Zhang, *Sci. Rep.* **4**, 6525 (2014).
- B. Hermann, M. Liu, N. Schmitner, B. Maurer, D. Meyer, W. J. Weninger, and W. Drexler, *Proc. SPIE* **9323**, 93232N (2015).
- L. Li, C. Dai, Q. Li, Q. Zhao, X. Jiang, X. Chai, and C. Zhou, *Opt. Lett.* **40**, 4448 (2015).
- X. Liu, T. Liu, R. Wen, Y. Li, C. A. Puliafito, H. F. Zhang, S. Jiao, R. Wen, T. Liu, H. F. Zhang, X. Liu, C. A. Puliafito, Y. Li, T. Liu, R. Wen, Y. Li, C. A. Puliafito, H. F. Zhang, and S. Jiao, *Opt. Lett.* **40**, 1370 (2015).
- D. Lee, C. Lee, S. Kim, Q. Zhou, J. Kim, and C. Kim, *Sci. Rep.* **6**, 35176 (2016).
- X. Shu, M. Bondu, B. Dong, A. Podoleanu, L. Leick, and H. F. Zhang, *Opt. Lett.* **41**, 2743 (2016).
- X. Liu, R. Wen, Y. Li, and S. Jiao, *J. Opt.-UK* **18**, 064001 (2016).
- S. Shang, Z. Chen, Y. Zhao, S. Yang, and D. Xing, *Opt. Express* **25**, 530 (2017).
- B. Dong, C. Sun, and H. F. Zhang, *IEEE Trans. Biomed. Eng.* **64**, 4 (2017).
- Z. Chen, S. Yang, Y. Wang, and D. Xing, *Opt. Lett.* **40**, 2838 (2015).
- Z. Chen, S. Yang, and D. Xing, *Opt. Lett.* **41**, 1636 (2016).
- T. Berer, E. Leiss-Holzinger, A. Hochreiner, J. Bauer-Marschallinger, and A. Buchsbaum, *J. Biomed. Opt.* **20**, 046013 (2015).
- P. Hajireza, K. Krause, M. Brett, and R. Zemp, *Opt. Express* **21**, 6391 (2013).
- P. Hajireza, J. Sorge, M. Brett, and R. Zemp, *Opt. Lett.* **40**, 1350 (2015).
- Y. Shu, X. Guo, M. Liu, and T. Buma, *IEEE Int. Ultra. Sym.* (2011), pp. 2349–2352.
- H. Li, B. Dong, Z. Zhang, H. F. Zhang, and C. Sun, *Sci. Rep.* **4**, 4496 (2014).
- K. Sathiyamoorthy, E. M. Strohm, and M. C. Kolios, *J. Biomed. Opt.* **22**, 046001 (2017).
- X. Zhu, Z. Huang, G. Wang, W. Li, D. Zou, and C. Li, *Opt. Lett.* **42**, 439 (2017).
- P. H. HajiReza, K. L. Bell, W. Shi, and R. J. Zemp, *Proc. SPIE* **10064**, 1006420 (2017).
- S. Preisser, W. Rohringer, M. Liu, C. Kollmann, S. Zotter, B. Fischer, and W. Drexler, *Biomed. Opt. Express* **7**, 4171 (2016).
- W. Qi, T. Jin, J. Rong, H. Jiang, and L. Xi, *J. Biophoton.* (2017).
- S. Ye, R. Yang, J. Xiong, K. K. Shung, Q. Zhou, C. Li, and Q. Ren, *Biomed. Opt. Express* **3**, 360 (2012).